remote sensing

MDPI

Article

Mapping Vegetation Changes in Mongolian Grasslands (1990–2024) Using Landsat Data and Advanced Machine Learning Algorithm

Mandakh Nyamtseren [1], Tien Dat Pham [2,3,*], Thuy Thi Phuong Vu [4], Itgelt Navaandorj [1] and Kikuko Shoyama [5]

[1] Institute of Geography-Geoecology, Mongolian Academy of Sciences, Ulaanbaatar 13330, Mongolia; n.mandakh@gmail.com (M.N.); itgelt0203@gmail.com (I.N.)
[2] School of Natural Sciences, Faculty of Science and Engineering, Macquarie University, Sydney, NSW 2109, Australia
[3] Hawkesbury Institute for the Environment, Western Sydney University, Richmond, NSW 2753, Australia
[4] Forest Inventory and Planning Institute (FIPI), Ministry of Agricultural and Rural Development (MARD), Vinh Quynh, Thanh Tri, Hanoi 100000, Vietnam; vuphuongthuyfipi@gmail.com
[5] College of Agriculture, Ibaraki University, Ami 300-0393, Japan; kikuko.shoyama.sx68@vc.ibaraki.ac.jp
* Correspondence: tiendat.pham@mq.edu.au or dat.pham@westernsydney.edu.au

Abstract: Grassland ecosystems provide a range of services in semi-arid and arid regions. However, they have significantly declined due to overgrazing and desertification. In the current study, we employed Landsat time series data (TM, OLI, OLI-2) spanning from 1990 to 2024, combined with vegetation indices such as NDVI and SAVI, along with NDWI and digital elevation models (DEMs), to analyze land cover dynamics in the Ugii Lake watershed area, Mongolia. By integrating multisource remote sensing data into the advanced XGBoost (extreme gradient boosting) machine learning algorithm, we achieved high classification accuracy, with overall accuracies exceeding 94% and Kappa coefficients greater than 0.92. The results revealed a decline in montane grasslands (−6.2%) and an increase in other grassland types, suggesting ecosystem redistribution influenced by climatic and anthropogenic factors. Cropland exhibited resilience, recovering from a significant decline in the 1990s to moderate growth by 2024. Our findings highlight the stability of barren land and underscore pressures from ecological degradation and human activities. This study provides up-to-date statistical data to support decision-making in the conservation and sustainable management of grassland ecosystems in Mongolia under changing climatic conditions.

Keywords: grassland; remote sensing; Landsat; XGBoost; Mongolia; vegetation change

check for updates

Academic Editors: Yuanwei Qin, Wei Cao and Jun Zhai

Received: 17 December 2024
Revised: 9 January 2025
Accepted: 22 January 2025
Published: 24 January 2025

Citation: Nyamtseren, M.; Pham, T.D.; Vu, T.T.P.; Navaandorj, I.; Shoyama, K. Mapping Vegetation Changes in Mongolian Grasslands (1990–2024) Using Landsat Data and Advanced Machine Learning Algorithm. *Remote Sens.* **2025**, *17*, 400. https://doi.org/10.3390/rs17030400

1. Introduction

Mongolia is considered a country with limited water resources, and the Government of Mongolia has prioritized the conservation, protection, and sustainable management of vegetations through laws, programs, and the implementation of an international obligation. Mongolian vegetation, particularly grassland ecosystems, provides valuable socio-economic and ecosystem resources for communities and native wildlife. These ecosystems play an important role as potential carbon sinks, contributing to the mitigation of global climate change [1].

In recent decades, Mongolian grasslands have been intensively utilized for livestock grazing, resulting in land degradation [2,3]. Another driver of land degradation is desertification, which has been exacerbated by climate change [4]. Grasslands across the country have significantly declined [5], resulting in reduced livestock yields, increased economic losses, increased vulnerabilities, and reduced living standards for rural communities [6]. In response, Mongolia has implemented significant policy measures, including sustainable grazing practices through rotational grazing systems and restrictions on overgrazing in sensitive areas. Large-scale land restoration programs, such as the Green Belt Initiative, focus on the reforestation and rehabilitation of degraded lands, supported by international collaborations, including the United Nations Convention to Combat Desertification (UNCCD) [7]. These efforts highlight the urgency of employing monitoring tools using Earth observations to track vegetation dynamics and inform effective policy interventions. Addressing these issues requires comprehensive, up-to-date vegetation databases to support sustainable land management.

Earth observations have been widely used for mapping vegetation, using various multispectral sensors, such as MODIS [8–10], Landsat TM, ETM+, OLI [11–14], Sentinel-2 [15–17], and PlanetScope [18], as well as synthetic aperture radar (SAR) sensors such as Sentinel-1 C-band [19,20]. SAR data are dependent on cloud cover and vegetation canopy. However, Sentinel-1 temporal data were not available before 2015, and their short wavelength is often sensitive to certain grassland types, making it challenging to distinguish them from forest and crop types [20]. On the other hand, optical sensors have been proven to be suitable for effectively mapping and monitoring vegetation changes in semi-arid and arid lands, as they offer lower costs and easier repeatability and cover wider areas [9,21]. The literature review shows that the methods used to map and detect decadal changes in drylands are diverse, ranging from those based on the Normalized Difference Vegetation Index (NDVI) [10,22] to pixel-based and object-based approaches [23,24].

NDVI-based approaches, commonly used for vegetation monitoring, leverage the contrast between near-infrared and red reflectance to quantify vegetation greenness. These methods are computationally efficient and suitable for long-term time-series analysis, especially in data-scarce regions. However, NDVI is sensitive to soil background effects and atmospheric conditions, which can distort vegetation assessments in arid and semi-arid regions. Persistent cloud cover also poses significant challenges in obtaining clear satellite images, limiting the temporal resolution and accuracy of such indices [25]. Additionally, NDVI-based methods primarily rely on temporal changes in vegetation indices but are often inefficient and incapable in automating change detection.

In contrast, object-based approaches utilize both spectral and spatial information from high-resolution imagery to segment and classify land cover. These methods are more suitable for analyzing heterogeneous landscapes [26] and address some of the limitations of pixel-based NDVI by incorporating contextual information. Nevertheless, object-based methods are computationally intensive and require substantial ground truth data for validation, which are often unavailable in remote regions, such as Mongolia's grasslands. Object-based approaches utilize spectral information about different vegetation types and relationships derived from optical remotely sensed data, enabling the automated monitoring of vegetation changes when multi-temporal Earth observations are available [9,27]. To overcome these challenges, integrating multisource data, such as digital elevation models (DEMs) and additional spectral indices, can enhance the accuracy of vegetation mapping and the detection of vegetation changes [28]. However, to the best of our knowledge, up-to-date grassland maps and their change detection using time-series Landsat (TM/OLI/OLI-2) imagery between 1990 and 2024 have not yet been reported for Mongolia. Thus, this study aims to fill the gap in the current literature by (1) investigating an advanced machine learning algorithm to map multi-decadal vegetation dynamics using Landsat time-series data between 1990 and 2024 in Mongolia, (2) providing up-to-date statistical analysis of areas of grassland areas in Mongolia for the first time in 2024 using Landat-9 OLI-2 as an important national grassland database, and (3) providing a valuable tool for decision-makers in supporting sustainable grassland conservation and management in Mongolia.

We hypothesis that integrating multi-source Earth observation data into advanced machine learning algorithms will produce accurate maps and a reliable database of multi-decadal grassland vegetation changes, providing insights for sustainable grassland management under changing climatic conditions.

2. Materials and Methods

2.1. Study Area

Ugii Lake in Mongolia (Figure 1) is a crucial wetland and a designated Ramsar site, hosting a diverse range of bird species, including the whooper swan, swan goose, and common pochard. The lake is also home to species with significant conservation status according to the IUCN Red List, such as the vulnerable saker falcon and the globally endangered steppe eagle. Additionally, species like the white-naped crane are classified as 'Rare' under Mongolian law [29].

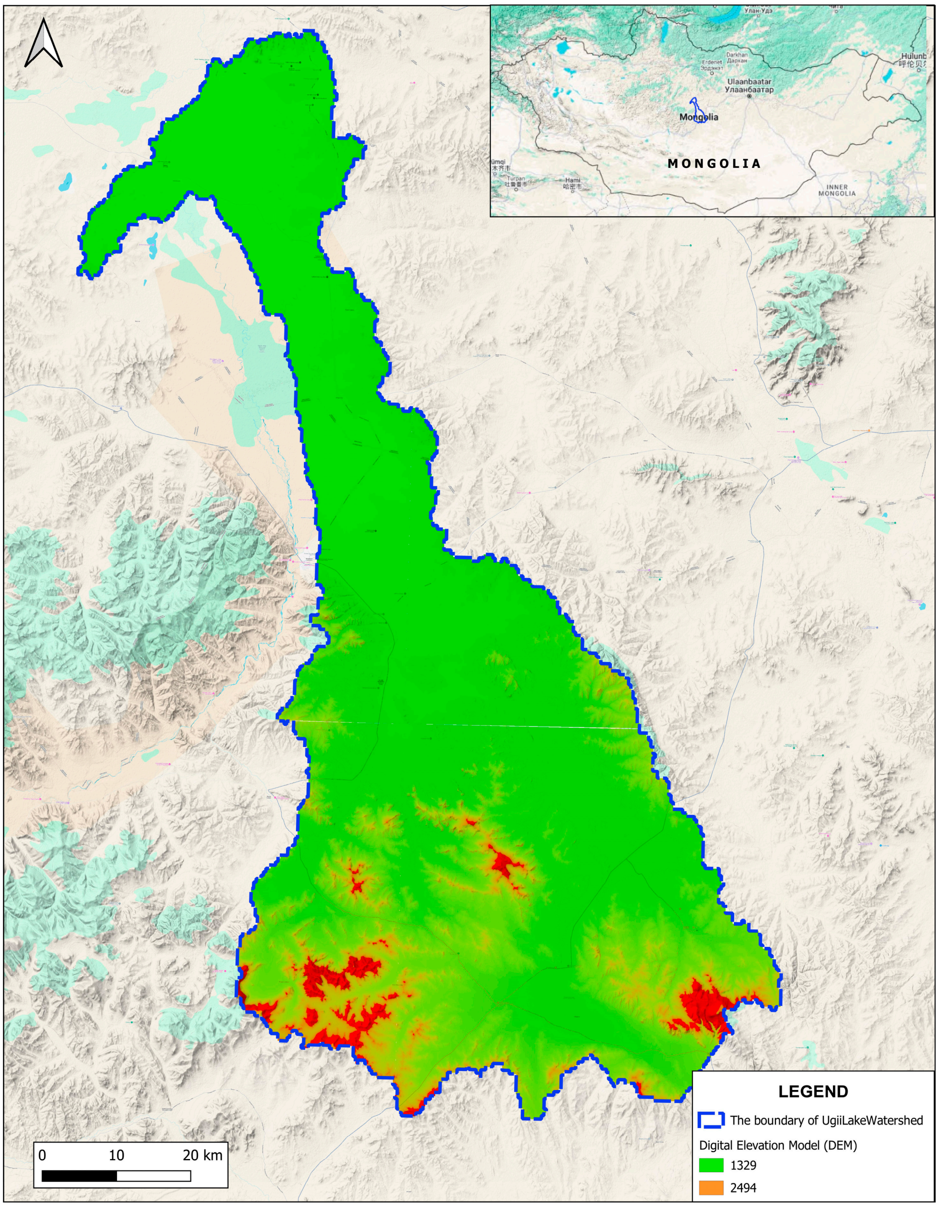

Figure 1. Location map of the study area at Ugii Lake in Mongolia.

Ugii Lake is also a popular tourist destination, attracting approximately 150,000 visitors annually. The primary land uses in the area include traditional livestock breeding, tourism, and infrastructure development [30]. However, the lake faces several environmental threats, including wetland degradation due to overgrazing, deforestation, and climate change. Invasive alien species further threaten the ecosystem, leading to habitat destruction and biodiversity loss. The lake and its surrounding grasslands support diverse vegetation types, including montane grasslands, meadow grasslands, and mixed grass species such as *Stipa* spp., *Leymus* spp., and *Artemisia* spp. Over the past three decades, these grasslands have undergone significant changes. Montane grasslands have declined, driven by overgrazing and climate-induced stressors, while meadow grasslands have shown some recovery in recent years due to reduced grazing pressures and natural regrowth [31].

Climate change has exacerbated issues such as droughts and altered ecological behaviors, impacting both local livelihoods and the environment. Furthermore, there is a significant lack of scientific research and monitoring of vegetation in the lake, leading to the poor management and overexploitation of resources, particularly in areas used for pastoralism and forestry [31,32].

2.2. Materials

Satellite Data

Multi-decadal Landsat surface reflectance (SR) data obtained through Earth explorer (https://earthexplorer.usgs.gov/, accessed on 1 October 2024) were used to map vegetation dynamics in the study area (Table 1). We used Collection 2, which were atmospherically corrected SR data with a single-channel algorithm developed by National Aeronautics and Space Administration (NASA) Jet Propulsion Laboratory (JPL). All data used in the current study (Table 1) were acquired from Landsat time-series Collection 2 SR.

Table 1. Time-series Landsat imagery used, covering 34 years in the study area.

Sensor	Spatial Resolution (m)	Image_ID	Cloud Cover (%)	Year	Band Used
Landsat-5 TM	30	LT05_L2SP_133027_19900908 LT05_L2SP_133028_19900908 LT05_L2SP_134027_19900916	2.0 0.0 2.0	1990	Coastal, Blue, Green, Red, Near-infrared (NIR), Mid-infrared (MIR), Shortwave infrared 1 (SWIR 1), Shortwave infrared 2 (SWIR 2)
Landsat-5 TM	30	LT05_L2SP_133027_20000919 LT05_L2SP_133028_20000919 LT05_L2SP_134027_20000926	1.0 0.0 3.0	2000	
Landsat-8 OLI	30	LC08_L2SP_133027_20200926 LC08_L2SP_133028_20200926 LC08_L2SP_134027_20200917	0.1 3.2 0.1	2020	
Landsat-9 OLI-2	30	LC09_L2SP_133027_20240812 LC09_L2SP_133028_20240812 LC09_L2SP_134027_20240819	0.0 0.7 0.0	2024	

Considering the seasonal changes in grasslands, we selected the summer season in September. To minimize the effects of cloud, datasets with less than 5% cloud coverage were acquired for the period from 1990 to 2024. We computed a mosaic of three Landsat scenes using ArcGIS Pro's Mosaic Dataset tool to cover the study area by applying histogram matching for relative radiometric normalization to ensure consistent radiometric properties, such as brightness, contrast, and reflectance values, across the input images.

The Advanced Land Observing Satellite Digital Surface Model (DSM) at a horizontal resolution of 30 m was used to map vegetation changes in grassland ecosystems within the study area (https://www.eorc.jaxa.jp/ALOS/en/dataset/aw3d30/index.htm, accessed on 1 October 2024).

2.3. Methods

2.3.1. Generation of Training and Validation Datasets for the Study Area

Ground-reference data points were selected through an initial visual spectral inspection of the very high spatial resolution images in Google Earth Pro (2024). Field surveys conducted in the study area in 2023 and 2024 were used to assess the spectral signatures of each land cover type identified through the visual inspection of multiple band compositions. Ground-reference points were located in the field using a Garmin handheld GPS with an accuracy of ± 2 m. At each reference point, the grass species present and their relative abundances were estimated and recorded.

For each class, the reference points guided the digitization of training samples. To enhance the spectral variability of class signatures, at least 500 samples were digitized for each class in the immediate vicinity of the ground reference locations. We employed the Segment Anything Model (SAM), which is an innovative segmentation model by Meta AI [33], to assist in the selection of training sets for past images. This toolset is available in QGIS as suggested by Ha et al. [34].

In this study, the training and the validation data were obtained from very high spatial resolution images in Google Earth Pro (2024), as suggested by [27], combining with visual interpretation after running the SAM. A total of 56,209 points were randomly selected. Table 2 shows the number of land cover classes and ground reference data samples digitized for creating the training and validation sets in the study area. We have adopted 12 classifications as the land use cover categories necessary in assessing ecosystem services in Mongolia. Specifically, classifying the five types of grassland is crucial in monitoring changes in the ecosystem of the target area and making policy recommendations.

Table 2. Vegetation classes determined from ground reference data and the number of digitized training samples using the SAM.

Class Name	Number of Samples
Barren	972
Cropland	4045
Urban/residential areas	143
Meadow grass	2491
Montane (*Stipa* + *Sedge* + *Artermisia*)	3496
Mix grasses (*Stipa* + *Artermisia* + *Leymus*)	4773
Tall grass (*Achnaterum*)	2453
Shrubland (*Caragana microphylla*)	1728
Forest	1645
Open forest	6315
Bogland	1935
Water bodies	4538

2.3.2. Computation of Spectral Indices

We computed three vegetation indices using Landsat (5/8/9) images as suggested by [2]. They are the Normalized Difference Vegetation Index (NDVI) (Equation (1)), Soil--Adjusted Vegetation Index (SAVI) (Equation (2)), and Normalized Difference Water Index (NDWI) (Equation (3)). The equations for the spectral indices are listed below:

$$\text{NDVI} = \frac{\rho_{nir} - \rho_{red}}{\rho_{nir} + \rho_{red}} \tag{1}$$

$$\text{SAVI} = (1 + L) \times \frac{\rho_{nir} - \rho_{red}}{\rho_{nir} + \rho_{red} + L} \tag{2}$$

$L = 0.5$ in most conditions

$$\text{NDWI} = \frac{\rho_{swir1} - \rho_{nir}}{\rho_{swir1} + \rho_{nir}} \tag{3}$$

where ρ_{red}, ρ_{green}, and ρ_{nir} are the surface reflectances for the red (band 3 for TM or band 4 for OLI and OLI-2), green (TM band 2 or OLI/OLI-2 band 3), and near-infrared (NIR: TM band 4 or OLI/OLI-2 band 5) bands, respectively.

2.3.3. Machine Learning Algorithm Development

We developed a machine learning model, which integrates six multispectral bands, three spectral indices, and DEM into the supervised extreme gradient boosting (XGB) algorithm, to automatically monitor vegetation ecosystems in Mongolia.

Extreme gradient boosting (XGB) [35] is currently the most widely used boosting method that employs ensemble-based decision tree learning and works effectively for both classification and regression problems. The XGB algorithm uses the theory of boosting techniques and belongs to the ensemble-based decision tree learning family. Initially introduced by Chen and Guestrin [6], XGB has been effectively applied in both classification and regression tasks in supervised learning domains [36].

In the XGB model, the two regularization terms L_1 and L_2 were added to the cost functions to improve generalization, optimize performance, and reduce the overfitting problem. For the XGB benchmark, several hyperparameters such as the booster type, a maximum depth, a minimum child weight, the number of trees, and a learning rate had to be set and tuned beforehand. The hyperparameters that were ultimately selected for the XGB model included the GBTREE booster, a learning rate of 0.01, a maximum depth of 5, a minimum child weight of 1, and a total of 1000 estimators (trees). Additionally, the subsample ratio and column sample by tree were both set to 0.8. The regularization parameters were specified as $L_1 = 0.01$ and $L_2 = 1.0$. We optimized hyperparameter for the XGB algorithm using a GridSearch with 5-fold cross-validation as suggested by [36].

To evaluate the effectiveness of the proposed model, we compared its performance with other ensemble learning algorithms, including Random Forests (RFs) [37] and Light Gradient-Boosting Machine (LGBM) [38]. Model development and comparison were conducted using Python 3.6 in a Jupiter Notebook environment. The machine learning models were implemented using libraries from Scikit-learn [39] and the LGBM package, available at https://lightgbm.readthedocs.io/en/stable/, accessed date 1 October 2024.

The hyperparameters for the RF model were optimized, including 1000 trees, a maximum depth of 10, and a maximum of 10 features. For the LGBM model, the boosting type was set to GBTREE, the learning rate was 0.05, the maximum depth was -1, the number of leaves was set to 100, and the number of trees was 500.

2.3.4. Decadal Maps of Vegetation Changes

We propose a framework that integrates multisource remote sensing datasets with advanced machine learning algorithms to map vegetation and grassland ecosystems and detect changes using time-series Landsat images from 1990 to 2024, as shown in Figure 2.

Change detection was conducted using pixel-based approaches through the standard confusion matrix tool in the ArcGIS Pro version 3.2 [40]. Analyzing the changes in the pairs of classified maps between 1990 and 2000 and between 2000 and 2024 using confusion matrix shows the loss, gain, and lack of change in grassland and other land use types.

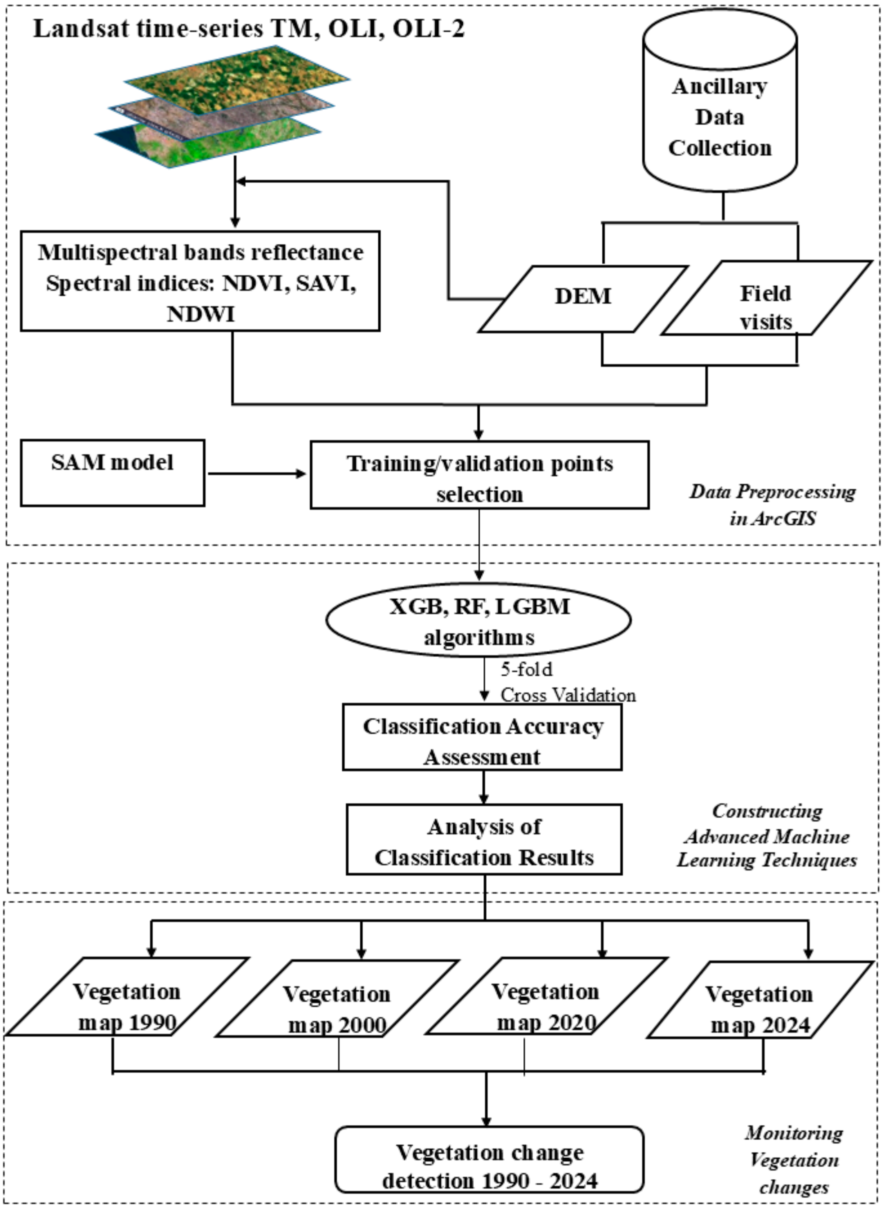

Figure 2. Proposed flowchart used to monitor vegetation changes in this study.

2.3.5. Accuracy Assessment

To ensure the reliability of classification models, we ran a procedure 5 times with 5-fold cross validation (CV) using 1000 trees and 10 features as inputs for three ensemble learning algorithms. The model produces data for the overall accuracy (OA) and Kappa coefficient, together with the F_1 score, precision, and recall. The model also performs the variable importance to assess the prediction accuracy and indicate the contribution of each variable. The overall accuracy (OA) and Kappa coefficient, together with the F_1 score, precision, and recall, were computed using the cross-validation procedure to evaluate the model performance.

A number of standard metrics, including the overall accuracy (OA) (Equation (4)), Kappa coefficient (κ) (Equation (5)), precision (Equation (6)), recall (Equation (7)), and the F_1 score (Equation (8)), were used to evaluate the effectiveness of the supervised classification [41,42].

$$OA\left(y, y_{pred}\right) = \frac{1}{n_{samples}} \sum_{i=0}^{n_{samples}-1} 1\left(y_{predi} = y_i\right) \tag{4}$$

in which

y_{pred} is the predicted value;
y_i is the corresponding true value;
$n_{samples}$ is the total number of validation samples.

$$\kappa = \frac{p_o - p_e}{1 - p_e} \tag{5}$$

in which

p_o is the observed agreement;
p_e is the expected agreement.

$$P = \frac{(TP)}{(TP) + (FP)} \tag{6}$$

$$R = \frac{(TP)}{(TP) + (FN)} \tag{7}$$

$$F_1 = 2 \times \frac{P \times R}{P + R} \tag{8}$$

in which

TP is a true positive;
FP is a false positive;
FN is a false negative.

2.3.6. Analysis and Statistical Method

The vegetation distribution maps and the grassland statistical areas for the study sites were computed using ArcGIS Pro Version 3.2 software to calculate the spatial distribution of grasslands in Mongolia.

3. Results

3.1. Performance of the RF, XGB, and LGBM Models Using Ground Truthing Data for 2024 Data

Table 3 compares the performance of three ensemble-based decision tree learning algorithms for mapping vegetation in Mongolian grasslands. All three algorithms demonstrated satisfactory results across standard matrices, including the overall accuracy (OA), Kappa coefficient (K), precision (P), recall (R), and F_1 score. The XGB model performed well and outperformed both the RF and the LGBM models, with an F_1 score reaching 0.95, an OA exceeding 94.92%, and a K of 0.92, indicating superior accuracy assessment in grassland classification. The RF model slightly underperformed compared to the LGBM model, achieving an OA of 94.17%, a K of 0.91, and an F_1 score of 0.94.

Table 3. Model performance for grassland detection at Ugii Lake, Mongolia.

Model	Overall Accuracy (%)	Kappa Coefficient	P	R	F_1
RF	94.17	0.91	0.94	0.94	0.94
XGB	94.92	0.92	0.95	0.95	0.95
LGBM	92.60	0.88	0.92	0.93	0.92

As XGB performed best, it was employed to make classification maps for the years 1990, 2000, 2020, and 2024.

3.2. Vegetation Classification and Accuracy Assessment

Our proposed approach, which integrated multisource Earth observations into the XGB algorithm, demonstrates superior overall accuracy in vegetation monitoring in Mongolia grasslands, achieving exceptional classification results, with an OA exceeding 94% and K coefficients greater than 0.92 (Table 4). As can be seen from Table 4, Landsat-9 OLI-2 produced slightly better results than Landsat-8 OLI, highlighting the success of the recently launched Landsat mission.

Table 4. Comparison of accuracy in monitoring vegetation in grasslands in the study area.

Year	Overall Accuracy (%)	Kappa Coefficient
1990 (Landsat-5 TM)	96.96	0.95
2000 (Landsat-5 TM)	96.66	0.96
2020 (Landsat-8 OLI)	94.08	0.92
2024 (Landsat-9 OLI-2)	94.92	0.92

Table 5 shows the classification results for each class between 1990 and 2024. Overall, the XGB algorithm successfully classified meadows, montane grasslands, tall grass types, and shrubs, including various dominant species such as *sedge*, *Artemisia Stipa*, *Artemisa*, *Leymus*, and *Caragana* spp., achieving F_1 scores greater than 0.9.

Table 5. Classification results for each class from 1990 to 2024 using multi-source data with the XGB algorithm.

Class Name	1990			2000			2020			2024		
	P	R	F_1 Score	P	R	F_1 Score	P	R	F_1 Score	P	R	F_1 Score
Barren	0.89	0.79	0.84	0.94	0.82	0.88	0.91	0.72	0.80	0.91	0.78	0.84
Cropland	0.99	1.00	1.00	0.99	1.00	0.99	0.97	0.99	0.98	0.98	0.99	0.99
Urban	0.94	0.90	0.92	0.95	0.83	0.89	0.90	0.69	0.78	0.94	0.68	0.79
Meadow grassland (*sedge* + *Artemisia*)	0.94	0.88	0.91	0.95	0.93	0,94	0.95	0.85	0.89	0.94	0.90	0.92
Montane grassland	0.92	0.95	0.94	0.94	0.97	0.96	0.88	0.90	0.89	0.86	0.85	0.85
Grassland (*Stipa* + *Artemisa* + *Leymus*)	0.93	0.90	0.92	0.96	0.96	0.96	0.91	0.90	0.90	0.88	0.88	0.88
Tall grass (*Achnaterum*)	0.94	0.96	0.95	0.97	0.97	0.97	0.94	0.97	0.95	0.90	0.87	0.89
Shrubland (*Caragana microphylla* + *Caragana pygmane*)	0.96	0.93	0.94	0.95	0.96	0.95	0.91	0.87	0.89	0.87	0.86	0.87
Forest	0.90	0.83	0.87	0.93	0.87	0.90	0.90	0.75	0.82	0.80	0.60	0.62
Open forest	0.90	0.93	0.91	0.93	0.96	0.94	0.87	0.94	0.91	0.86	0.95	0.90
Bog	0.97	0.97	0.97	0.99	0.99	0.99	0.97	0.97	0.97	0.97	0.98	0.97
Water bodies	1.00	1.00	1.00	1.00	0.99	1.00	0.99	0.99	0.99	1.00	1.00	1.00

The results underscore the effectiveness of advanced machine learning classification-based approaches for detailed land use analysis and grasslands dynamics, emphasizing the importance of Landsat-time series data, particularly the new Landsat-9 OLI-2, in mapping vegetation in grasslands in semi-arid and arid regions.

3.3. Vegetation Dynamics from 1990 to 2024

Figure 3 shows the spatial distribution of vegetation and grassland ecosystems in the Ugii Lake watershed area, Mongolia, over the 34 years between 1990 and 2024.

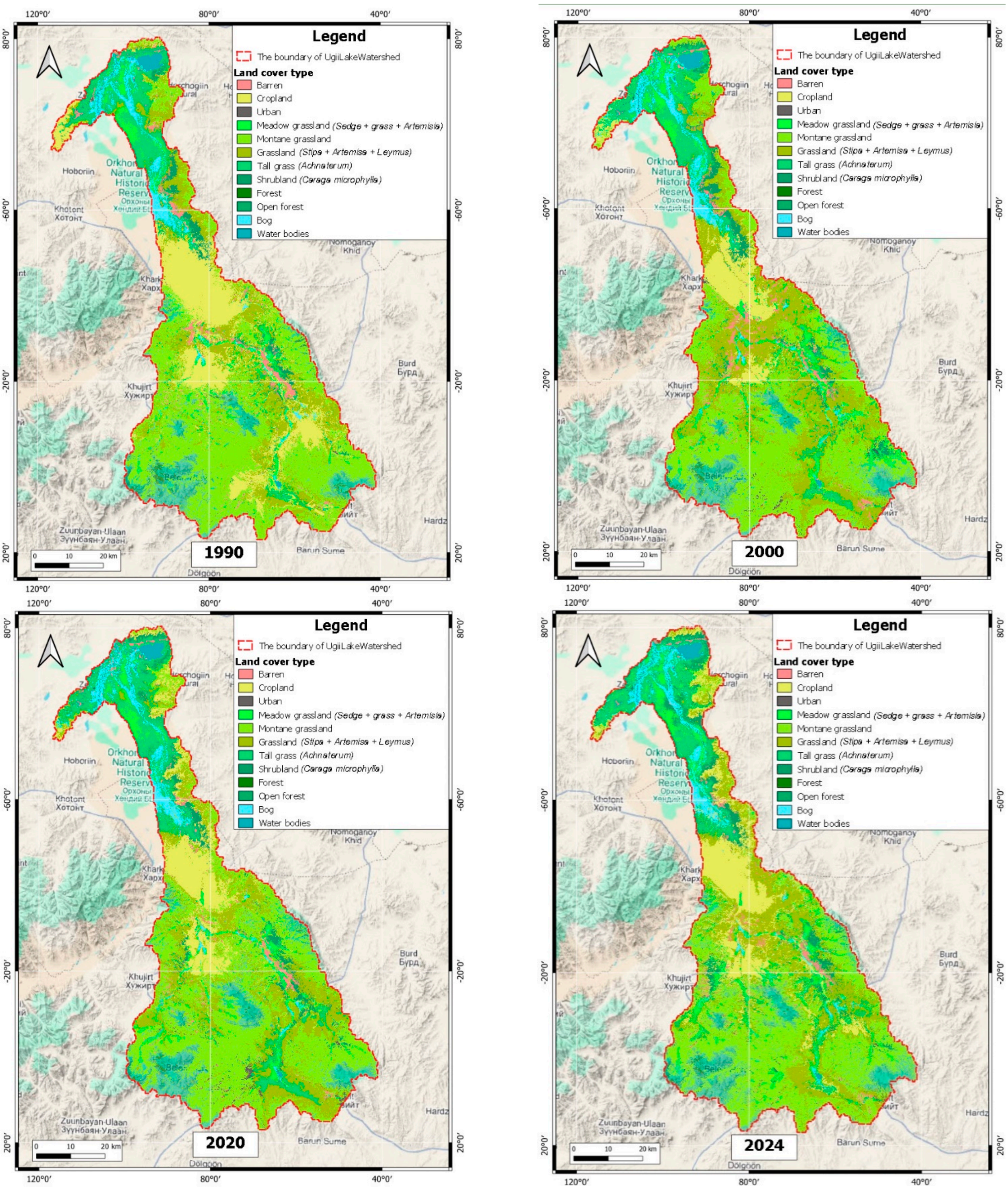

Figure 3. Maps of vegetation and grassland types between 1990 and 2024.

The analysis of land cover changes over the period 1990–2024 highlights significant spatial and temporal transformations in various land cover classes. The cropland class experienced a sharp decline from 18.8% in 1990 to 7.0% in 2000, followed by recovery to 9.9% in 2020 and 13.3% in 2024. The class of montane grassland remained relatively stable until 2020 (36.7% in 1990 to 38.3% in 2020) but showed a significant reduction to 32.1% by 2024.

Figures 4 and 5 illustrate that urban areas grew steadily from 0.2% in 1990 to 0.7% in 2020, before declining to 0.3% in 2024, suggesting a reversal in urban sprawl or the reclassification of land. Grasslands (mainly composed of *Stipa* spp., *Artemisia* spp., and *Leymus* spp.) increased significantly from 16.5% in 1990 to 24.6% in 2000, followed by a reduction to 19.1% in 2020 and recovery to 20.6% in 2024, reflecting fluctuations in ecological or anthropogenic drivers. The change analysis showed that from 1990 to 2000, dramatic shifts were observed, particularly in cropland (−11.8%) and grassland (+8.1%), suggesting significant land use changes during this period. From 2000 to 2020, moderate recovery was evident in cropland (+2.9%), while montane grassland (+2.1%) exhibited slight growth, potentially due to improved management practices. From 2020 to 2024, montane grassland declined sharply (−6.2%), indicating accelerated degradation, whereas meadow grassland showed slight recovery (+1.7%).

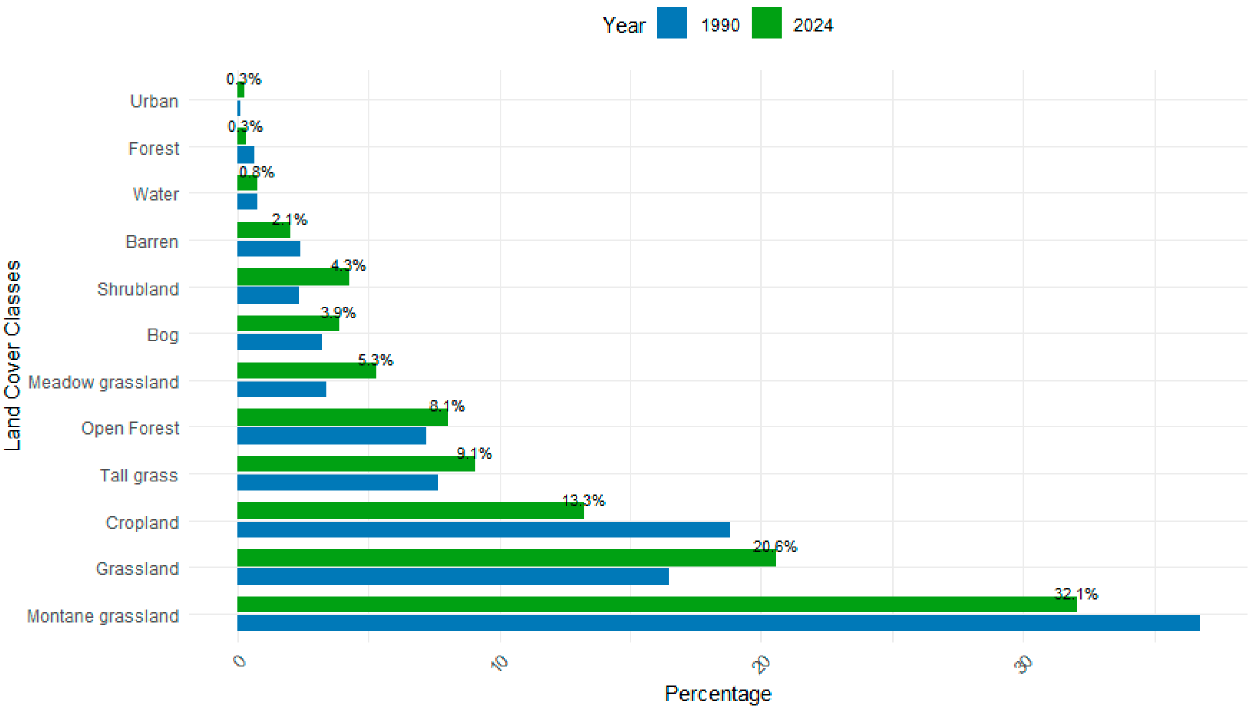

Figure 4. Land cover types as percentages of the total land.

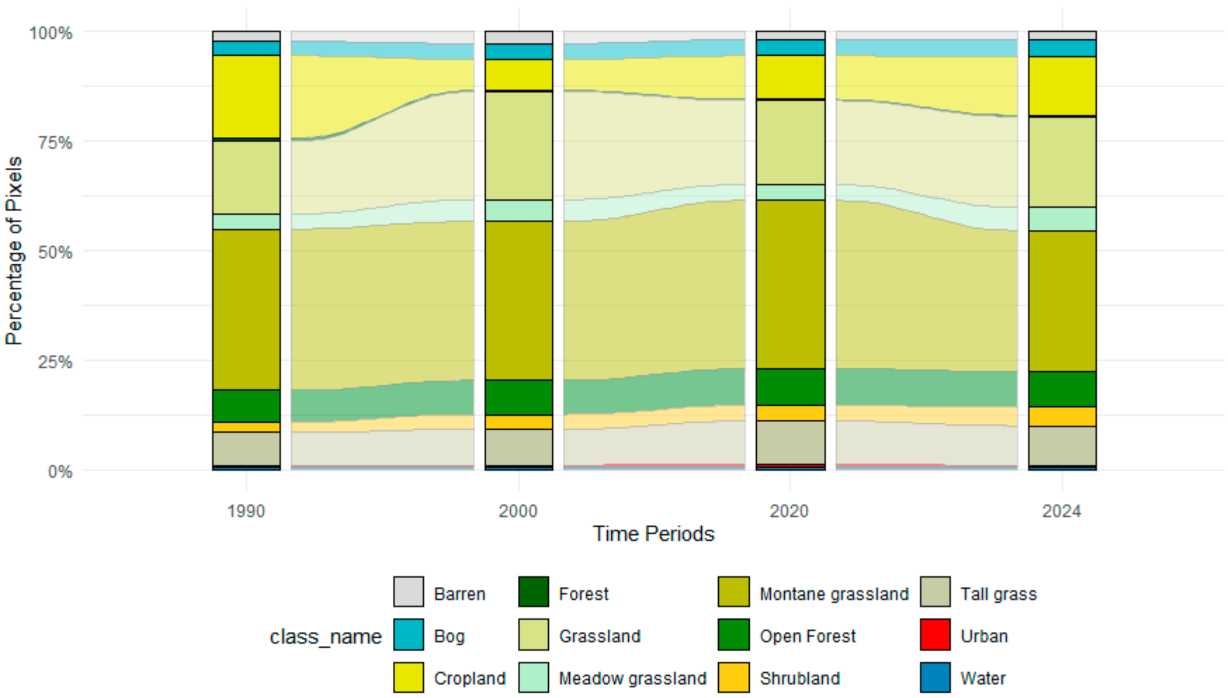

Figure 5. Sankey diagrams showing land cover changes from 1990 to 2024.

Figure 6 illustrates the spatial vegetation dynamics from 1990 to 2024 in the Ugii Lake watershed area, Mongolia.

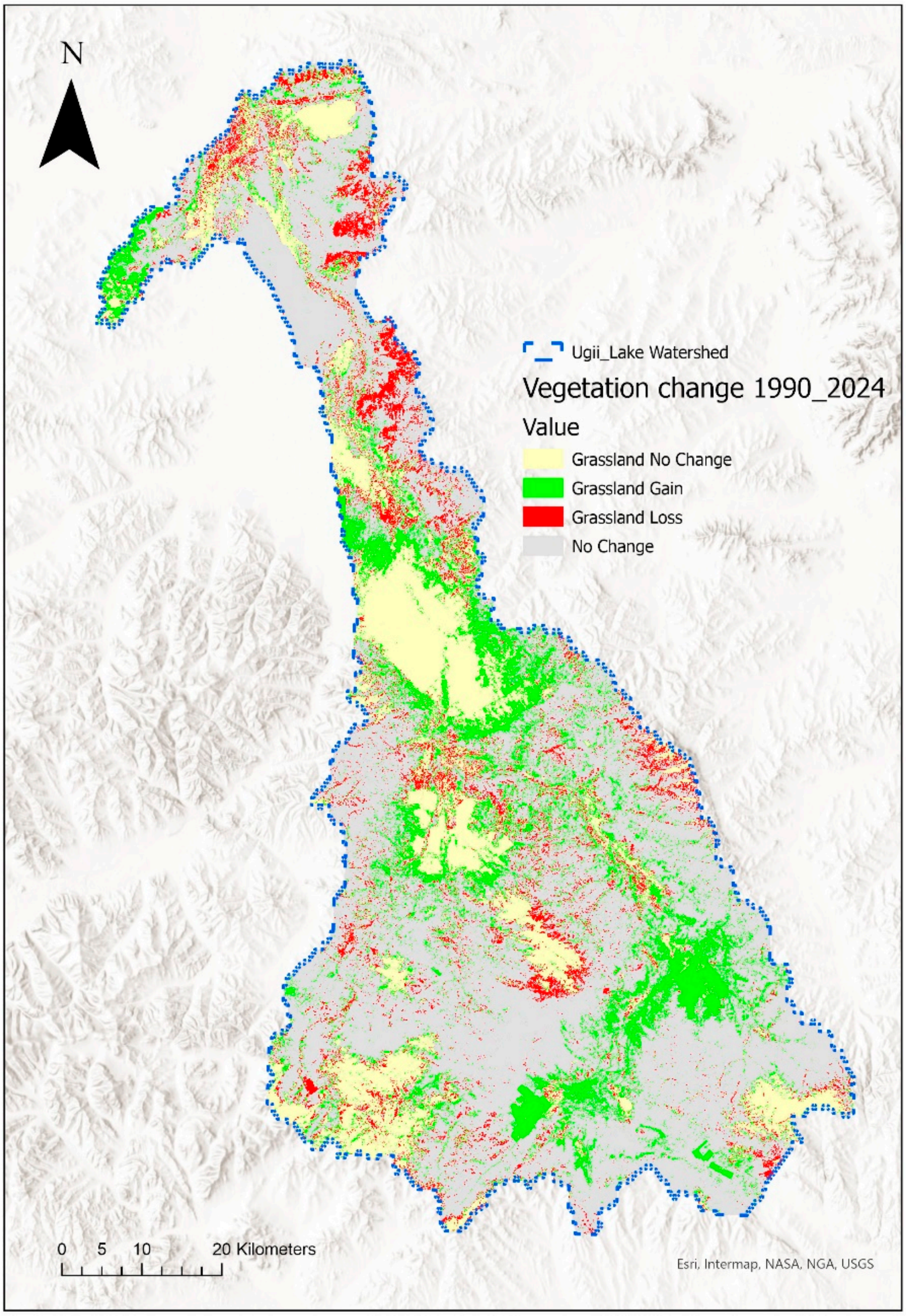

Figure 6. Vegetation dynamics at Ugii Lake, Mongolia.

Overall, the period reflects contrasting trends, with montane grassland declining and other grassland types increasing, indicating the redistribution of ecosystems. Despite initial urban growth, the overall changes in urban areas were minimal, likely due to limited urban expansion in the study area. Cropland demonstrated resilience, rebounding from early losses, possibly due to shifts in land use policies or agricultural intensification. The decline in montane grassland and the stability of barren land highlights pressures from ecological degradation or human activities.

4. Discussion

4.1. Advanced Machine Learning Approach to Vegetation Mapping in Grasslands and Change Detection

Our proposed approach, which integrates multisource Earth observation data from multispectral bands, spectral indices, and DEM into an advanced ensemble decision tree learning technique, achieved superior classification results for vegetation mapping in Mongolian grasslands, with overall accuracies exceeding 94% and Kappa coefficients greater than 0.92. Our results show that the XGB algorithm yielded the highest performance and outperformed other ensembled decision learning algorithms, i.e., the RF and the LGBM models. One possible reason is that XGB uses the boosting technique and implements both L_2 and L_1 regularization to prevent overfitting and ensure robustness, whereas RF lacks explicit regulation, relying more on bagging for variance reduction [28].

Our results surpass recent grassland classification efforts, such as using the RF algorithm with Landsat-8 OLI data with an accuracy of 88.3 [12], MODIS NDVI data with an overall accuracy of 72.17% [10], and 20 years of MODIS datasets with accuracies ranging from 81% to 91% [9], as well as surpassing the overall accuracy ranging from 80% to 95% achieved using PlanetScope data [3].

Our results underscore the effectiveness of advanced machine learning-based approaches for the detailed classification of various dominant species, including *sedge*, *Artemisia Stipa*, *Artemisa*, *Leymus*, and *Caragana* spp., achieving F_1 scores greater than 0.9. This highlights the importance of Landsat time-series data over 24 years (1990–2024), particularly the new Landsat-9 OLI-2, for mapping grassland ecosystems in semi-arid and arid regions. Importantly, up-to-date grassland statistics were obtained with high precision and reliability by combining Landsat data with the XGB algorithm.

Our study further highlights that selecting point samples using the SAM Segmentation algorithm, with boundary constraints for similar grasslands, cropland, and forests, is key in achieving high accuracy when ground truthing data are limited. The effectiveness of the SAM algorithm has also been corroborated by recent studies [33,43].

4.2. Drivers of Vegetation Changes from 1990 to 2024

The observed changes in land cover are likely influenced by a combination of ecological and anthropogenic drivers. For example, the decline in cropland during the 1990s aligns with economic and policy transitions following Mongolia's move to a market economy, which disrupted traditional agricultural practices [6]. The subsequent recovery of cropland by 2024 may reflect the impact of targeted agricultural intensification programs [44]. Similarly, the increase in grasslands during the 1990s could be attributed to land abandonment and ecological succession, a trend observed in post-Soviet states [8]. However, the sharp decline in montane grasslands after 2020 is likely driven by overgrazing, desertification, and climatic stressors, such as reduced precipitation and rising temperatures [5]. Urban expansion, although modest, underscores the gradual shift toward infrastructure development in rural areas, a pattern also evident in other arid and semi-arid regions worldwide [45].

The vegetation change dynamics in grasslands observed in the Ugii Lake region of Mongolia align with broader trends reported in Mongolian and global studies. The significant decline in montane grasslands (−6.2% from 2020 to 2024) reflects findings reported by Hilker et al. [5], who attributed widespread grassland degradation in Mongolia to overgrazing and precipitation variability, exacerbated by climate impacts such as increasing temperatures and aridity, as highlighted in the *Mongolia Assessment Report on Climate Change* [46].

Fluctuations in cropland, characterized by a sharp decline from 1990 to 2000 (−11.8%) followed by partial recovery by 2024 (+6.3%), reflect broader land use changes in post-

Soviet states, driven by policy shifts and changing agricultural priorities. Urban dynamics, showing modest growth followed by a decline, suggest limited urban expansion in rural Mongolia, likely due to the predominantly nomadic lifestyle. Overall, these trends underscore the interplay between anthropogenic factors, such as overgrazing and agricultural practices, and climatic drivers, including temperature increases and precipitation variability. These findings are consistent with Addison et al. [45], who critically reviewed land degradation assumptions and emphasized the significant influence of socio-economic and ecological pressures in Mongolian rangelands.

Importantly, our results provide reliable database for assessing the current status of grasslands in the Ugii Lake region of Mongolia and offer valuable insights into leveraging multisource Earth observation data and machine learning for grassland monitoring in semi-arid and arid land regions.

4.3. Implications for Sustainable Grassland Conservation and Management in the Context of Climate Change

Our results have significant implications for grassland conservation and management in the context of climate change. The decline in montane grasslands underscores the urgent need for targeted interventions, such as sustainable grazing practices and habitat restoration, to mitigate land degradation. Grasslands are vital carbon sinks and biodiversity reservoirs; their degradation threatens ecosystem services while exacerbating the impacts of climate change [45].

The recovery observed in certain vegetation classes, such as meadow grasslands, highlights opportunities for adaptive management strategies that harness natural regenerative processes. Policymakers should prioritize the integration of ecological monitoring tools into conservation planning to enhance resilience in grassland ecosystems [47]. Furthermore, incorporating remote sensing data for large-scale monitoring into decision-making processes can significantly improve the precision of conservation efforts, particularly in regions with limited field data availability [48,49].

4.4. Current Limitations and Future Research Directions

Although this study achieved high accuracy in mapping vegetation dynamics using 30 m temporal Landsat time-series data, several limitations remain. First, reliance on satellite imagery introduces potential biases due to atmospheric effects, such as cloud cover and haze, as well as the radiometric calibration of mosaic images using histogram matching, which can affect image quality [50,51]. Incorporating alternative data sources, such as SAR imagery from Sentinel-1 and ALOS PALSAR, could help mitigate these challenges, enhance temporal coverage, and enable the phenology-based monitoring of grasslands.

Second, the study's dependence on field-based ground truth data meant that it was constrained by accessibility in remote regions. Since ground truth data collection is time-consuming and costly, particularly for large grassland areas in semi-arid and arid lands, future research should focus on the development of advanced machine learning techniques, such as self-supervised [52,53] and semi-supervised learning [54,55], to reduce dependency on extensive ground truth data.

Finally, although this study focused on Mongolian grasslands, the proposed methodology has broader applicability to semi-arid and arid regions worldwide. Expanding this approach to other regions could offer valuable comparative insights and validate its robustness across diverse ecological contexts. Future studies should also consider integrating geographical, socio-economic, and institutional variables to better understand the drivers of vegetation dynamics and support integrated land management strategies in the context of changing climates.

5. Conclusions

In this research, we integrated multisource Earth observation data into advanced ensemble decision tree learning techniques to map and detect vegetation changes in Mongolian grasslands. We compared three ensemble-based decision tree learning algorithms for supervised classification. Our results showed superior accuracy for all techniques, with the XGB model outperforming the others, achieving an overall accuracy of 94.92% and precision, recall, and F_1 scores of 0.95.

We applied the XGB model to multi-temporal Landsat data to detect grassland cover types over a 34-year period from 1990 to 2024 in the Ugii Lake region. Our analysis revealed notable changes in grasslands, including a decline in montane grasslands and an increase in other grassland types. This study provides valuable insights that can support sustainable grassland conservation and management efforts in Mongolia in the context of climate change.

Author Contributions: Conceptualization, T.D.P. and K.S.; methodology, T.D.P., T.T.P.V. and M.N.; software, T.D.P. and M.N.; validation, T.D.P. and K.S.; formal analysis, T.D.P., T.T.P.V. and I.N.; investigation, M.N. and I.N.; resources, T.D.P., K.S. and M.N.; data curation, T.D.P. and M.N.; writing—original draft preparation, T.D.P., M.N. and K.S.; writing—review and editing, T.D.P., I.N., and K.S.; visualization, T.D.P., T.T.P.V. and K.S.; supervision, K.S.; project administration, K.S.; funding acquisition, K.S. All authors have read and agreed to the published version of the manuscript.

Funding: This research was funded by the Asian Pacific Network for Global Change Research APN, grant number CRRP2022-02MY-Shoyama.

Data Availability Statement: The original contributions presented in this study are included in the article. Further inquiries can be directed to the corresponding author.

Acknowledgments: The authors would like to thank the Institute of Geography-Geo-ecology, Mongolian Academy of Sciences, for assistance during the field surveys in 2023 and 2024. The authors would like to thank local authorities for their generous assistance during the fieldwork and technical data process. T.D.P. is supported by a Macquarie University Research Fellowship (Grant No. MQRF0001124-2021).

Conflicts of Interest: The authors declare no conflicts of interest.

References

1. Reading, R.P.; Bedunah, D.; Amgalanbaatar, S. Conserving Mongolia's Grasslands, with Challenges, Opportunities, and Lessons for North America's Great Plains. *Great Plains Res.* **2010**, *20*, 85–107.
2. Na, Y.; Li, J.; Hoshino, B.; Bao, S.; Qin, F.; Myagmartseren, P. Effects of Different Grazing Systems on Aboveground Biomass and Plant Species Dominance in Typical Chinese and Mongolian Steppes. *Sustainability* **2018**, *10*, 4753. [CrossRef]
3. Dashpurev, B.; Wesche, K.; Jäschke, Y.; Oyundelger, K.; Phan, T.N.; Bendix, J.; Lehnert, L.W. A cost-effective method to monitor vegetation changes in steppes ecosystems: A case study on remote sensing of fire and infrastructure effects in eastern Mongolia. *Ecol. Indic.* **2021**, *132*, 108331. [CrossRef]
4. Guo, X.; Chen, R.; Thomas, D.S.G.; Li, Q.; Xia, Z.; Pan, Z. Divergent processes and trends of desertification in Inner Mongolia and Mongolia. *Land Degrad. Dev.* **2021**, *32*, 3684–3697. [CrossRef]
5. Hilker, T.; Natsagdorj, E.; Waring, R.H.; Lyapustin, A.; Wang, Y. Satellite observed widespread decline in Mongolian grasslands largely due to overgrazing. *Glob. Change Biol.* **2014**, *20*, 418–428. [CrossRef]
6. Goodland, A.; Sheehy, D.; Shine, T. *Mongolia Livestock Sector Study, Volume I–Synthesis Report*; Sustainable Development Department, East Asia and Pacific Region, World Bank: Washington, DC, USA, 2009.
7. Volodya, E.; Yeo, M.J.; Kim, Y.P. Trends of Ecological Footprints and Policy Direction for Sustainable Development in Mongolia: A Case Study. *Sustainability* **2018**, *10*, 4026. [CrossRef]
8. Yin, H.; Pflugmacher, D.; Li, A.; Li, Z.; Hostert, P. Land use and land cover change in Inner Mongolia—Understanding the effects of China's re-vegetation programs. *Remote Sens. Environ.* **2018**, *204*, 918–930. [CrossRef]
9. Phan, T.-N.; Dashpurev, B.; Wiemer, F.; Lehnert, L.W. A simple, fast, and accurate method for land cover mapping in Mongolia. *Geocarto Int.* **2022**, *37*, 14432–14450. [CrossRef]

10. Meng, B.; Zhang, Y.; Yang, Z.; Lv, Y.; Chen, J.; Li, M.; Sun, Y.; Zhang, H.; Yu, H.; Zhang, J.; et al. Mapping Grassland Classes Using Unmanned Aerial Vehicle and MODIS NDVI Data for Temperate Grassland in Inner Mongolia, China. *Remote Sens.* **2022**, *14*, 2094. [CrossRef]
11. Meng, X.; Gao, X.; Li, S.; Li, S.; Lei, J. Monitoring desertification in Mongolia based on Landsat images and Google Earth Engine from 1990 to 2020. *Ecol. Indic.* **2021**, *129*, 107908. [CrossRef]
12. Reece, N.; Wingard, G.; Mandakh, B.; Reading, R.P. Using Random Forest to Classify Vegetation Communities in the Southern Area of Ikh Nart Nature Reserve in Mongolia. *Mong. J. Biol. Sci.* **2019**, *17*, 31–39.
13. Price, K.P.; Guo, X.; Stiles, J.M. Optimal Landsat TM band combinations and vegetation indices for discrimination of six grassland types in eastern Kansas. *Int. J. Remote Sens.* **2002**, *23*, 5031–5042. [CrossRef]
14. Liu, M.; Qu, Y.; Wang, J.; Liao, Y.; Zheng, G.; Guo, Y.; Liu, L. A 30-m annual grassland dataset from 1991 to 2020 for Inner Mongolia, China. *Sci. Data* **2024**, *11*, 1143. [CrossRef]
15. Phiri, D.; Simwanda, M.; Salekin, S.; Nyirenda, V.R.; Murayama, Y.; Ranagalage, M. Sentinel-2 Data for Land Cover/Use Mapping: A Review. *Remote Sens.* **2020**, *12*, 2291. [CrossRef]
16. Mohammadpour, P.; Viegas, D.X.; Viegas, C. Vegetation Mapping with Random Forest Using Sentinel 2 and GLCM Texture Feature—A Case Study for Lousã Region, Portugal. *Remote Sens.* **2022**, *14*, 4585. [CrossRef]
17. Hill, M.J. Vegetation index suites as indicators of vegetation state in grassland and savanna: An analysis with simulated SENTINEL 2 data for a North American transect. *Remote Sens. Environ.* **2013**, *137*, 94–111. [CrossRef]
18. Andreatta, D.; Gianelle, D.; Scotton, M.; Dalponte, M. Estimating grassland vegetation cover with remote sensing: A comparison between Landsat-8, Sentinel-2 and PlanetScope imagery. *Ecol. Indic.* **2022**, *141*, 109102. [CrossRef]
19. Tuvdendorj, B.; Zeng, H.; Wu, B.; Elnashar, A.; Zhang, M.; Tian, F.; Nabil, M.; Nanzad, L.; Bulkhbai, A.; Natsagdorj, N. Performance and the Optimal Integration of Sentinel-1/2 Time-Series Features for Crop Classification in Northern Mongolia. *Remote Sens.* **2022**, *14*, 1830. [CrossRef]
20. Norovsuren, B.; Tseveen, B.; Batomunkuev, V.; Renchin, T. Estimation for forest biomass and coverage using Satellite data in small scale area, Mongolia. *IOP Conf. Ser. Earth Environ. Sci.* **2019**, *320*, 012019. [CrossRef]
21. Pham, T.D.; Ha, N.T.; Saintilan, N.; Skidmore, A.; Phan, D.C.; Le, N.N.; Viet, H.L.; Takeuchi, W.; Friess, D.A. Advances in Earth observation and machine learning for quantifying blue carbon. *Earth-Sci. Rev.* **2023**, *243*, 104501. [CrossRef]
22. Valderrama-Landeros, L.; Flores-de-Santiago, F.; Kovacs, J.M.; Flores-Verdugo, F. An assessment of commonly employed satellite-based remote sensors for mapping mangrove species in Mexico using an NDVI-based classification scheme. *Environ. Monit. Assess.* **2017**, *190*, 23. [CrossRef] [PubMed]
23. Pham, T.D.; Xia, J.; Ha, N.T.; Bui, D.T.; Le, N.N.; Takeuchi, W. A Review of Remote Sensing Approaches for Monitoring Blue Carbon Ecosystems: Mangroves, Seagrassesand Salt Marshes during 2010–2018. *Sensors* **2019**, *19*, 1933. [CrossRef]
24. Silveira, E.M.O.; Silva, S.H.G.; Acerbi-Junior, F.W.; Carvalho, M.C.; Carvalho, L.M.T.; Scolforo, J.R.S.; Wulder, M.A. Object-based random forest modelling of aboveground forest biomass outperforms a pixel-based approach in a heterogeneous and mountain tropical environment. *Int. J. Appl. Earth Obs. Geoinf.* **2019**, *78*, 175–188. [CrossRef]
25. West, H.; Quinn, N.; Horswell, M. Remote sensing for drought monitoring & impact assessment: Progress, past challenges and future opportunities. *Remote Sens. Environ.* **2019**, *232*, 111291. [CrossRef]
26. Blaschke, T.; Hay, G.J.; Kelly, M.; Lang, S.; Hofmann, P.; Addink, E.; Queiroz Feitosa, R.; van der Meer, F.; van der Werff, H.; van Coillie, F.; et al. Geographic Object-Based Image Analysis—Towards a new paradigm. *ISPRS J. Photogramm. Remote Sens.* **2014**, *87*, 180–191. [CrossRef]
27. Vu, T.T.P.; Pham, T.D.; Saintilan, N.; Skidmore, A.; Luu, H.V.; Vu, Q.H.; Le, N.N.; Nguyen, H.Q.; Matsushita, B. Mapping Multi-Decadal Mangrove Extent in the Northern Coast of Vietnam Using Landsat Time-Series Data on Google Earth Engine Platform. *Remote Sens.* **2022**, *14*, 4664. [CrossRef]
28. Phan, D.C.; Trung, T.H.; Truong, V.T.; Sasagawa, T.; Vu, T.P.T.; Bui, D.T.; Hayashi, M.; Tadono, T.; Nasahara, K.N. First comprehensive quantification of annual land use/cover from 1990 to 2020 across mainland Vietnam. *Sci. Rep.* **2021**, *11*, 9979. [CrossRef] [PubMed]
29. Orkhonselenge, A.; Uuganzaya, M.; Davaagatan, T. Lake Ugii. In *Lakes of Mongolia: Geomorphology, Geochemistry and Paleoclimatology*; Orkhonselenge, A., Uuganzaya, M., Davaagatan, T., Eds.; Springer International Publishing: Cham, Switzerland, 2022; pp. 329–344. [CrossRef]
30. Orkhonselenge, A.; Uuganzaya, M.; Davaagatan, T. Touristic Prospects of Lakes in Mongolia. In *Lakes of Mongolia: Geomorphology, Geochemistry and Paleoclimatology*; Orkhonselenge, A., Uuganzaya, M., Davaagatan, T., Eds.; Springer International Publishing: Cham, Switzerland, 2022; pp. 423–441. [CrossRef]
31. Schwanghart, W.; Frechen, M.; Kuhn, N.J.; Schütt, B. Holocene environmental changes in the Ugii Nuur basin, Mongolia. *Palaeogeogr. Palaeoclimatol. Palaeoecol.* **2009**, *279*, 160–171. [CrossRef]

32. Sumiya, E.; Dorjsuren, B.; Yan, D.; Dorligjav, S.; Wang, H.; Enkhbold, A.; Weng, B.; Qin, T.; Wang, K.; Gerelmaa, T. Changes in water surface area of the lake in the Steppe Region of Mongolia: A case study of Ugii Nuur Lake, Central Mongolia. *Water* **2020**, *12*, 1470. [CrossRef]
33. Osco, L.P.; Wu, Q.; de Lemos, E.L.; Gonçalves, W.N.; Ramos, A.P.M.; Li, J.; Marcato, J. The Segment Anything Model (SAM) for remote sensing applications: From zero to one shot. *Int. J. Appl. Earth Obs. Geoinf.* **2023**, *124*, 103540. [CrossRef]
34. Ha, N.T.; Pham, T.D.; Tran, T.T.H. Zoning Seagrass Protection in Lap an Lagoon, Vietnam Using a Novel Integrated Framework for Sustainable Coastal Management. *Wetlands* **2021**, *41*, 122. [CrossRef]
35. Chen, T.; Guestrin, C. Xgboost: A scalable tree boosting system. In Proceedings of the 22nd ACM SIGKDD International Conference on Knowledge Discovery and Data Mining, San Francisco, CA, USA, 13–17 August 2016; pp. 785–794.
36. Le, N.N.; Pham, T.D.; Yokoya, N.; Ha, N.T.; Nguyen, T.T.T.; Tran, T.D.T.; Pham, T.D. Learning from multimodal and multisensor earth observation dataset for improving estimates of mangrove soil organic carbon in Vietnam. *Int. J. Remote Sens.* **2021**, *42*, 6866–6890. [CrossRef]
37. Breiman, L. Random Forests. *Mach. Learn.* **2001**, *45*, 5–32. [CrossRef]
38. Ke, G.; Meng, Q.; Finley, T.; Wang, T.; Chen, W.; Ma, W.; Ye, Q.; Liu, T.-Y. Lightgbm: A highly efficient gradient boosting decision tree. In Proceedings of the Advances in Neural Information Processing Systems, Long Beach, CA, USA, 4–9 December 2017; pp. 3146–3154.
39. Pedregosa, F.; Varoquaux, G.; Gramfort, A.; Michel, V.; Thirion, B.; Grisel, O.; Blondel, M.; Prettenhofer, P.; Weiss, R.; Dubourg, V. Scikit-learn: Machine learning in Python. *J. Mach. Learn. Res.* **2011**, *12*, 2825–2830.
40. van Duynhoven, A.; Dragićević, S. The Geographic Automata Tool: A New General-Purpose Geosimulation Extension for ArcGIS Pro. *Appl. Sci.* **2024**, *14*, 6530. [CrossRef]
41. Badreldin, N.; Prieto, B.; Fisher, R. Mapping Grasslands in Mixed Grassland Ecoregion of Saskatchewan Using Big Remote Sensing Data and Machine Learning. *Remote Sens.* **2021**, *13*, 4972. [CrossRef]
42. Wang, Z.; Ma, Y.; Zhang, Y.; Shang, J. Review of Remote Sensing Applications in Grassland Monitoring. *Remote Sens.* **2022**, *14*, 2903. [CrossRef]
43. Ren, Y.; Yang, X.; Wang, Z.; Yu, G.; Liu, Y.; Liu, X.; Meng, D.; Zhang, Q.; Yu, G. Segment Anything Model (SAM) Assisted Remote Sensing Supervision for Mariculture—Using Liaoning Province, China as an Example. *Remote Sens.* **2023**, *15*, 5781. [CrossRef]
44. Li, W.; Huntsinger, L. China's Grassland Contract Policy and its Impacts on Herder Ability to Benefit in Inner Mongolia. Tragic Feedbacks. *Ecol. Soc.* **2011**, *16*, 1. [CrossRef]
45. Addison, J.; Friedel, M.; Brown, C.; Davies, J.; Waldron, S. A critical review of degradation assumptions applied to Mongolia's Gobi Desert. *Rangel. J.* **2012**, *34*, 125–137. [CrossRef]
46. Dagvadorj, D.; Natsagadorj, L.; Dorjpurev, J.; Namkhainyam, B. MARCC 2009: Mongolia Assessment Report on Climate Change 2009. Available online: https://www.adaptation-undp.org/resources/mongolia-assessment-report-climate-change (accessed on 20 October 2024).
47. de Bello, F.; Lavorel, S.; Gerhold, P.; Reier, Ü.; Pärtel, M. A biodiversity monitoring framework for practical conservation of grasslands and shrublands. *Biol. Conserv.* **2010**, *143*, 9–17. [CrossRef]
48. Franke, J.; Keuck, V.; Siegert, F. Assessment of grassland use intensity by remote sensing to support conservation schemes. *J. Nat. Conserv.* **2012**, *20*, 125–134. [CrossRef]
49. Primi, R.; Filibeck, G.; Amici, A.; Bückle, C.; Cancellieri, L.; Di Filippo, A.; Gentile, C.; Guglielmino, A.; Latini, R.; Mancini, L.D.; et al. From Landsat to leafhoppers: A multidisciplinary approach for sustainable stocking assessment and ecological monitoring in mountain grasslands. *Agric. Ecosyst. Environ.* **2016**, *234*, 118–133. [CrossRef]
50. Zhang, Y.; Yao, Y.; Wan, Y.; Liu, W.; Yang, W.; Zheng, Z.; Xiao, R. Histogram of the orientation of the weighted phase descriptor for multi-modal remote sensing image matching. *ISPRS J. Photogramm. Remote Sens.* **2023**, *196*, 1–15. [CrossRef]
51. Wang, L.; Bai, Y.; Wang, J.; Zhou, Z.; Qin, F.; Hu, J. Histogram matching-based semantic segmentation model for crop classification with Sentinel-2 satellite imagery. *GIScience Remote Sens.* **2023**, *60*, 2281142. [CrossRef]
52. Milella, A.; Reina, G.; Underwood, J. A Self-learning Framework for Statistical Ground Classification using Radar and Monocular Vision. *J. Field Robot.* **2015**, *32*, 20–41. [CrossRef]
53. Wang, Y.; Albrecht, C.M.; Braham, N.A.A.; Mou, L.; Zhu, X.X. Self-Supervised Learning in Remote Sensing: A review. *IEEE Geosci. Remote Sens. Mag.* **2022**, *10*, 213–247. [CrossRef]
54. Bhullar, A.; Nadeem, K.; Ali, R.A. Simultaneous multi-crop land suitability prediction from remote sensing data using semi-supervised learning. *Sci. Rep.* **2023**, *13*, 6823. [CrossRef]
55. Yan, P.; He, F.; Yang, Y.; Hu, F. Semi-Supervised Representation Learning for Remote Sensing Image Classification Based on Generative Adversarial Networks. *IEEE Access* **2020**, *8*, 54135–54144. [CrossRef]